Stability and magnetism of hydrogen dimers on graphene

Yves Ferro,[1,*] D. Teillet-Billy,[2] N. Rougeau,[2] V. Sidis,[2] S. Morisset,[1] and Alain Allouche[1]

[1]*Laboratoire de Physique des Interactions Ioniques et Moléculaires, Université de Provence/CNRS-UMR 6633, Campus de Saint Jérôme, Services 242, 13397 Marseille Cedex 20, France*

[2]*Laboratoire des Collisions Atomiques et Moléculaires, Université Paris-Sud 11/CNRS-UMR 8625, Université Paris-Sud, Bât. 351, 91405 Orsay Cedex, France*

We report on the magnetism and stability of H dimers on a graphene sheet. Graphene is used as a simple model to grasp the basics of the H interaction with graphitic systems including graphite, graphene, polyaromatic hydrocarbons, and nanotubes. The dimers investigated here are found to be in ferromagnetic, antiferromagnetic, or nonmagnetic states. Results obtained from DFT calculations on the H dimer adsorption are analyzed with the help of spin-density maps. We thereby show that the dimer stability results from the magnetic properties of the pair of H atoms on graphene. The stability of dimers adsorbed in *ortho* and *para* positions is particularly emphasized. In order to rationalize the single and double H atom adsorption mechanisms, the whole pair formation process is divided into theoretical elementary steps to which energetic values are assigned.

　　　　　　　　　　　　PACS number(s): 73.20.Hb, 75.70.Ak

I. INTRODUCTION

The interaction of hydrogen with graphitic systems has attracted a sustained attention for the past nine years since the papers of Jeloaica and co-workers.[1,2] This work was originally concerned with the catalytic formation of molecular hydrogen in the interstellar medium. The number of domains of interest has since then kept on growing. It currently includes, among others, carbon nanoscience and nanotechnology applications as well as nuclear graphite (first walls of tokamaks).

The present work aims at investigating some key features of the adsorption, diffusion, and recombination processes of H atoms on graphitic systems for which numerous experimental results exist at the moment. The system under investigation is a single layer of graphite: a graphene sheet. This is a topic of particular interest for nanoscience applications. It is also a simple and efficient model to catch the essential features of the H-graphite interactions.

The present work focuses on the H dimers stability on graphene as resulting from the magnetic properties of the dimers. H atom adsorption is known to induce structural, electronic, and chemical modifications at the surface of graphite. Proton irradiation was also experimentally observed to produce magnetization as reported by Esquinazi *et al.*[3] Based on theoretical works, the defect-induced magnetism was shown to be a single H atom adsorbed on the surface,[4] hydrogen terminated step edges as model by nanographene[5] and nanoribbons,[6] or free terminated step edges.[7] The atomic vacancy is also able, in some cases, to lead to magnetism; this was theoretically investigated through density-functional theory (DFT) calculations in its nonmagnetic[8,9] and magnetic states;[4,10] the latter one being more stable by 0.1 eV.[11]

H dimers on a common carbon ring were recently shown to be in (↑↑) spin configuration when adsorbed in the *meta* position and in the (↑↓) spin configuration when adsorbed in the *ortho* and *para* positions (see Fig. 1 for the dimers

designation).[12] The so-called *ortho* and *para* dimers are known to be at the heart of the molecular hydrogen recombination mechanism, which is a crucial issue in the interstellar medium as well as in nuclear graphite. A previous experimental/theoretical study combining high-resolution electron energy-loss spectroscopy (HREELS) measurements and results of DFT calculations showed that H atom adsorption proceeds through the formation of stable H clusters composed of two to four H atoms.[13] Temperature programmed desorption (TPD) spectra of graphite at low D coverage show two main peaks[14,15] related to two different kinds of structures. Scanning tunneling microscope (STM) observations and STM image simulations from DFT calculations converge to the identification of these two stable structures as being the *ortho* and *para* dimers, the latter one leading to recombination into molecular hydrogen.[14]

We here investigate the H dimers stability and magnetism on graphene. We first focus on the magnetic state and spin density induced by a single H atom adsorption. The dimers stability is then shown to be predictable from the spin-
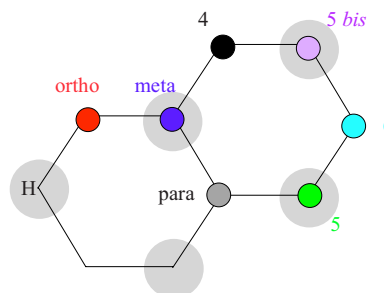

FIG. 1. (Color online) Configurations of the seven different H dimers. The first H is displayed on the figure, it is supposed to be adsorbed on an *A* type carbon atom (shaded circle). To form dimers, the second H atom is located on carbon atoms of different types in the *ortho*, *para*, *4*, and *6* positions. To form non-Kekule dimers it is located on same carbon atom types in the *meta*, *5*, and *5 bis* positions.

density map of this single event. Magnetic dimers are found to be in a ferromagnetic or antiferromagnetic spin configurations; these different spin polarizations are thoroughly investigated and the stability they induce is analyzed. These results are subsequently discussed with regard to those of Boukhvalov *et al.*[16] At last and in order to rationalize the single and double H atom adsorption mechanisms, the whole pair formation process is divided into theoretical elementary steps to which we assign energies of reaction. These data are designed to investigate the dynamics of the pair formation process as in kinetic Monte Carlo simulations.

II. COMPUTATIONAL METHODS AND MODELS

Periodic as well as cluster DFT calculations have been performed in the present work. Periodic calculations have been carried out with the ABINIT code,[17] based on the density-functional theory using the Perdew, Burke, and Ernzerhof gradient corrected generalized gradient approximation (GGA) functional for exchange and correlation.[18] A norm-conserving pseudopotential has been used to model the ionic core,[19] and the plane-wave basis set was given a cutoff energy of 25 hartree (680 eV). The Brillouin zone was sampled in a $3 \times 3 \times 1$ mesh using the Monkhorst-Pack scheme.[20] We have chosen a large 6×6 supercell to avoid any interaction between adsorption sites of neighboring supercells. Convergence was checked on the k-points mesh, energy cutoff, and size of the supercell. As in Ref. 8 the convergence is achieved at 6×6. The dimension of the hexagonal 2D unit cell was set to 2.42 Å. We have set the interlayer distance to 13.4 Å in order to avoid any interaction between graphene layers. While equivalent in the case of graphene, the two carbon atoms belonging to the unit cell are here labeled A and B as in graphite. The A and B carbon atoms are, respectively, located at the (0, 0) and (1/3, 2/3) reduced coordinates. The K corner of the Brillouin zone at the Fermi level of graphene connects two degenerate levels belonging to the π and π^* bands. The wave function associated with one degenerate level at K (the other degenerated level) involves all the A carbon atoms (the B carbon atoms) of the graphite layer;[8,21] it will be denoted as ϕ_A (ϕ_B) throughout.

The geometry of a single H atom adsorption was calculated optimized on a 3×3 supercell and then translated into a 6×6 one; this procedure was adopted owing to the huge computational demand of optimization runs in large supercell periodic calculations. As established in several previous works, among which those of Refs. 1, 2, 22, and 23, we find that the H atom adsorbs on top of a C atom of the graphene layer. This is the only stable H adsorption site on graphene. The adsorption geometry is at a distance $d_{\text{H graphene}}$ =1.518 Å and with an out-of-plane displacement of the adsorbent C atom by d_C=0.395 Å. The seven different configurations of the H dimers investigated in this paper are shown in Fig. 1. Except for the *ortho* dimer case, we build the geometry of the different dimers by translating $d_{\text{H graphene}}$ and d_C calculated for a single H atom on each adsorption site. This is supported by previous periodic slab and cluster calculations.[12,24] The *ortho* dimer was shown to have a different geometry. It is very similar to that of the (cis substi-
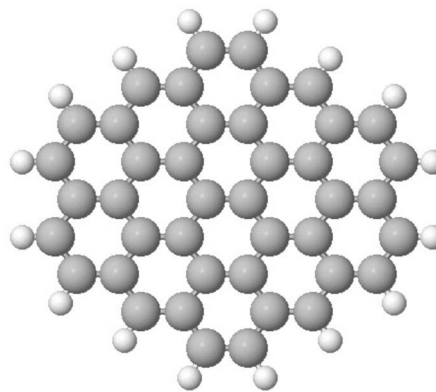

FIG. 2. "Circum pyrene" $C_{42}H_{16}$, the PAH type molecule presently used as a model of a graphene sheet.

tuted) ethane molecule;[12,14,24] it was determined on a 3×3 supercell and further translated into a 6×6 one. The ferromagnetic and antiferromagnetic electronic configurations were imposed by fixing the occupancies of the electronic bands in the spin-polarized calculations. Both ($\uparrow\uparrow$) and ($\uparrow\downarrow$) arrangements denote the spin configurations of the two highest occupied bands in the ferromagnetic and antiferromagnetic cases, respectively.

Solutions of the spin-polarized calculation with degenerate spin-up and spin-down levels and identical $\rho\uparrow$ and $\rho\downarrow$ are denoted as *restricted* in the following: these solutions lead to turn off magnetism since the spin density becomes zero everywhere in the supercell. In the other cases, the magnetic solutions are said to be *unrestricted*.

At last, calculations have been performed using no symmetry in order to allow broken-symmetry solutions of the Kohn-Sham equations. All the spin-density maps are calculated as the difference between the $\rho\uparrow$ and $\rho\downarrow$ densities and summed along the interlayer distance.

A molecular approach has also been used. The latter approach lends itself more readily to geometry optimizations. The cluster DFT calculations have been performed on polyaromatic hydrocarbons (PAH) type molecules; an example of which is shown in Fig. 2. These are known to constitute relevant models for H atom adsorption on graphitic surfaces.[1,22] In the cluster calculations both the H and adsorbent C were allowed to relax. The cluster calculations are based on the unrestricted Kohn-Sham DFT approach and are carried out with the ADF 2007 code.[25] Consistently with previous calculations,[12] the present ones are performed with inclusion of the PW91 (Ref. 26) generalized gradient correction of the exchange-correlation functional. PW91 and Perdew-Burke-Ernzerhof (PBE) were already shown to give consistent results as regard to H-graphite interaction.[1,2,4,12,13,16,22–24] We checked that for all the cases presently considered the cluster PBE adsorption results lie 5 ± 1 kJ/mol above the PW91 ones. The triple ζ+ polarization (TZP) basis of Slater-type orbitals provided with the ADF package was used. We previously checked[2] that there is no basis set superposition error (BSSE) with this basis. Cluster calculations were successfully used in Ref. 12 to investigate the *ortho*, *para*, and *meta* dimers in both spin paired ($\uparrow\downarrow$) and unpaired ($\uparrow\uparrow$) configurations. These calculations

TABLE I. Adsorption energies in kJ mol^{-1} calculated on (a) a 6×6 periodic model and (b) on a circum-pyrene $C_{42}H_{16}$ molecular model. (c) The magnetization in μ_B was calculated by summing the spin density over the whole supercell. (d) Electronic configuration as fixed by band occupancies (periodic calculations) or spin multiplicity (molecular calculations). U and R, respectively, refer to unrestricted and restricted Kohn-Sham solutions in the periodic calculations. All the molecular results are obtained in the unrestricted Kohn-Sham framework. (e) Calculated on a larger cluster to avoid border effects. (f) Nonmagnetic dimers. (sdm) Corresponding spin-density maps are shown in Figs. 3 and 4.

System	Mag$^{(c)}$	KS$^{(d)}$ solution	E_{ads} periodic$^{(a)}$	E_{ads} molecular$^{(b)}$
H graphite	1	↑-$U$$^{(sdm)}$	−67	−59
Ortho	0	↑↓-$R$$^{(f)}$	−229	−204
		↑↑-U		−150
Para	0	↑↓-$R$$^{(f)}$	−222	−203
		↑↑-U		−122
1–4	0	↑↓-$U$$^{(sdm)}$	−132	−102
	2	↑↑-U	−112	−94
1–6	0	↑↓-U$^{(sdm)}$	−163	−143$^{(e)}$
	2	↑↑-U	−110	−102$^{(e)}$
Meta	0	↑↓-U	−114	−103
	2	↑↑-$U$$^{(sdm)}$	−123	−109
1–5	0	↑↓-U	−107	−92
	2	↑↑-$U$$^{(sdm)}$	−119	−104
1–5 *bis*	0	↑↓-U	−114	−102
	2	↑↑-$U$$^{(sdm)}$	−128	−108

demonstrated the strong stabilization of the *ortho* and *para* dimers as compared to the *meta* ones for spin paired (↑↓) configurations; they also first showed the spin unpaired stabilization for *meta* dimers. This approach is presently used to study H dimers involving chemisorption on two remote positions.

III. RESULTS

Table I presents the adsorption energies of a single H atom and the seven H dimer adsorptions on a single layer of a graphitic surface. Both spin couplings (↑↑) and (↑↓) have been considered. The spin-density maps are plotted in Figs. 3 and 4; they display the spin density resulting from the adsorption of a single H atom and of dimers, respectively. Figure 3 is used to forecast the propensity of each site toward the adsorption of a second H atom. It can be considered as a visualization of the initial state prior to the second H atom adsorption. Figure 4 is used to analyze the final magnetic states formed after the second adsorption. It is most often consistent with the superposition of two single adsorption maps located at each adsorption site. These figures will be further discussed later on.

From Table I, the energy of adsorption of a single H atom is in good agreement with previous calculations.[1,22–24] On the other hand, deviations are observed in the comparison be-
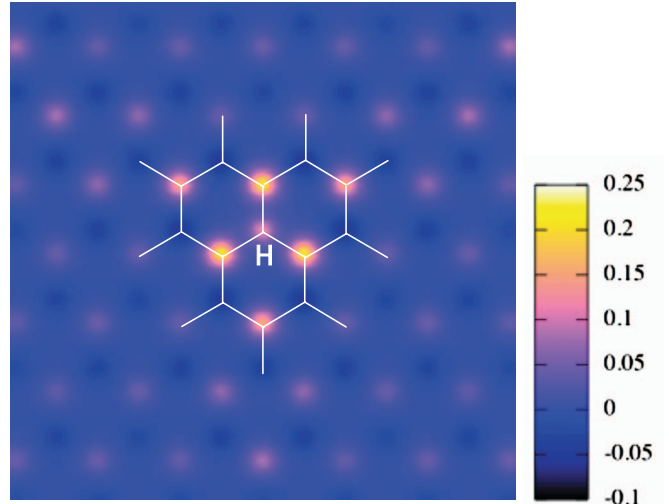

FIG. 3. (Color) Single H adsorption on a 6×6 supercell of graphene. Projected spin density onto the graphene plane.

tween molecular and periodic dimers adsorption energies: the molecular approach systematically underestimates the adsorption energies. This is clearly not a matter of choice of the GGA functional but rather a cluster effect. Nevertheless, both sets of molecular and periodic results are quite consistent in the sense that the same electronic configurations and the same relative dimer stabilities are found.

Ortho and *para* (↑↓) dimers are actually nonmagnetic (restricted solution); they exhibit strong stabilities as compared to other dimers or other electronic configurations. The mechanism through which stabilization occurs is further analyzed and discussed below.

A. Mesomeric effect

We first give a molecular description of a single H atom adsorption on an aromatic system. We then describe the preferential regio selectivity of the *ortho* and *para* sites for the second H atom adsorption; a reactivity which can qualitatively be explained by the so-called *mesomeric effect*.[27]

Figure 5 shows the adsorption of $H^•$ (with an unpaired electron) on an aromatic ring. The ring is tied to H atoms or others aromatic rings through *in-plane* bonds that are not displayed. The first H atom adsorption involves the breaking of one aromatic π bond. Once adsorbed, the unpaired electron or *radical* is delocalized at the *ortho* and *para* positions due to the mesomeric effect. Another $H^•$ will preferentially bind in those positions insuring electron pairing and formation of a stable C-H chemical bond. The system is then in a nonmagnetic singlet electronic configuration when in the ground state.

On the *meta* position, the formation of a chemical C-H bond implies breaking another aromatic π bond. This particular configuration is known as *non-Kekule* with the ground state in a triplet spin configuration (↑↑),[28,29] which induces a spin polarization of the ring.

B. Single H atom adsorption

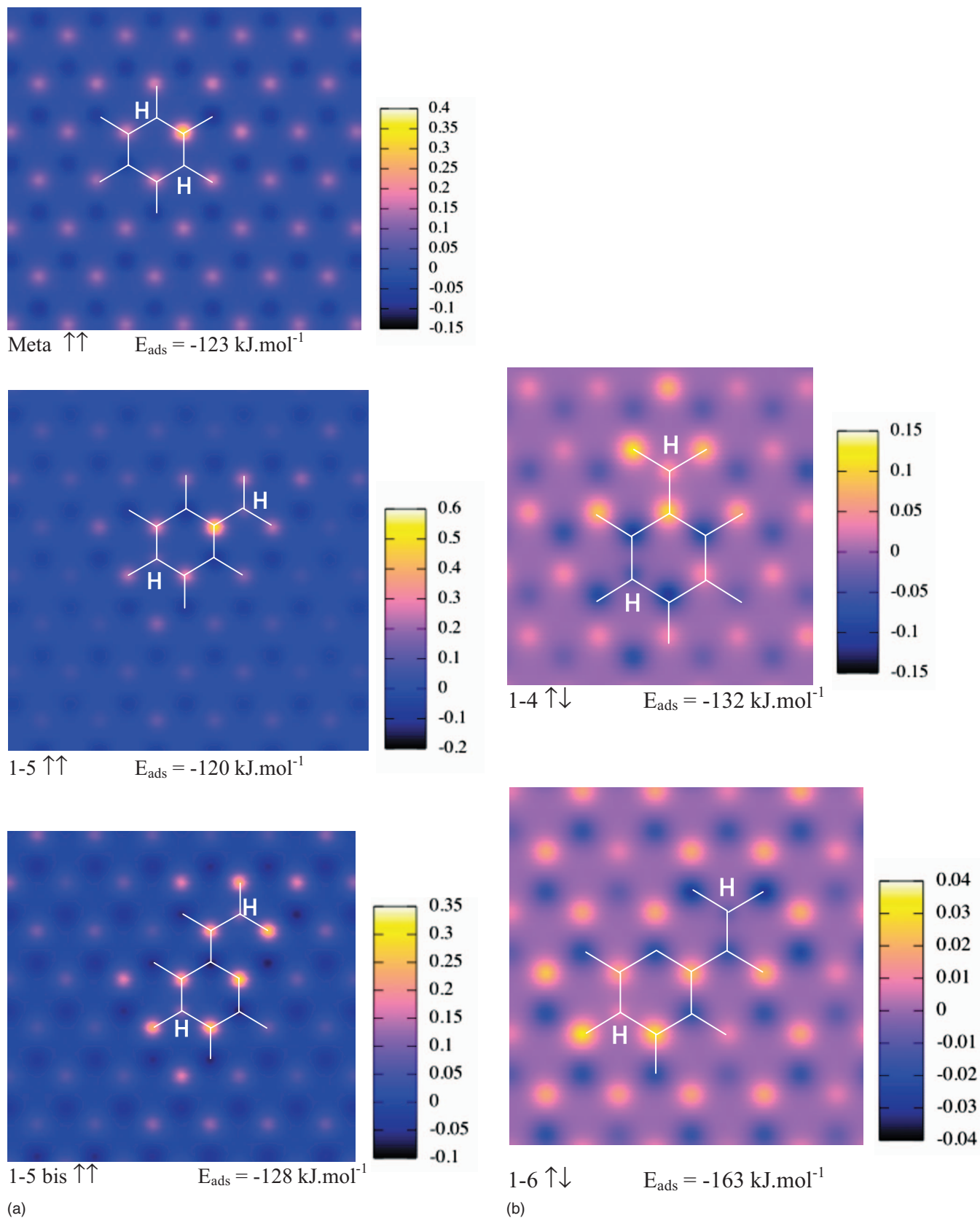Figure 3 displays the spin density resulting from of a single H atom adsorption. It is strongly localized around the

FIG. 4. (Color) (a) Non-Kekule: meta, 1–5, and 1–5 *bis*; (b) 1–4 and 1–6 dimers on a 6×6 supercell of graphene. Projected spin density onto the graphene plane.
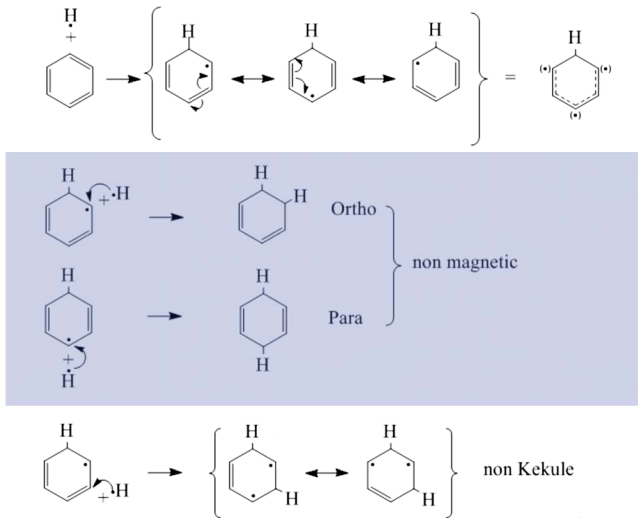
FIG. 5. (Color online) Double H adsorptions on an aromatic ring. Mesomeric effect and non-Kekule structures. The in-plane bonds are not shown. The C-H bonds resulting from the adsorption process, which are perpendicular to the ring plane, are drawn in the plane.

adsorption site. Assuming that H is adsorbed on an *A* carbon atom, the spin density is borne by all the *B* carbon atoms surrounding the adsorption site, and more particularly those in the *ortho* and *para* positions. The bare surface of graphite has a filled π level and an empty π^* one at the K corner. An *extra* electron in an empty ϕ_B orbital induces a spin density at all the *B* type carbon atoms. Assuming the H adsorption to be isolated on the infinite surface, the extra electron would be brought through the $1s_1$ orbital in a first approximation. Actually, the $1s$ orbital of H($1s_1$), filled with one electron, mixes with the empty ϕ_B orbital from the π^* band of graphite. This mixing has been previously investigated on a molecular (pyrene) cluster model.[30] As a result, a stable χ_{1B} orbital is formed, which is localized on H and on the *B* carbon atoms of the three aromatic rings to which H is bonded. These C atoms are in *ortho* and *para* positions with respect to the adsorption site as seen in Fig. 3. This picture is similar to the one obtained using the mesomeric effect on a molecular model; the mesomeric effect being just another way to take into account the structure of the wave function at the Fermi level.

This view aims at catching the essential features of the H-graphene interaction; however it only applies to a single H adsorption on an infinite surface. The periodic adsorption is more complex since the whole π and π^* bands interact with the $1s$ band from the H lattice. The resulting electronic band structure was found with the highest occupied band filled with electrons of same spin in a ferromagnetic configuration. However this band does not disperse as the result of the large supercell we choose insuring a good connection with an isolated adsorption. Such a supercell was also shown to be large enough to model an isolated atomic vacancy.[8]

C. The H dimers

1. Magnetism

Table I reports the dimers adsorption energies calculated for ferromagnetic, antiferromagnetic, and nonmagnetic con-

figurations. From these results, two behaviors may be drawn: When both H atoms are adsorbed on the same type of carbon atoms (for example: *meta*, 1–5, and 1–5 *bis*), the most stable electronic structure is in the ($\uparrow\uparrow$) arrangement and is thus ferromagnetic [Fig. 4(a)]; when the H atoms are adsorbed on different types of carbon atoms (for example *ortho*, *para*, 1–4, and 1–6 dimers) the ground state is in the ($\uparrow\downarrow$) arrangement. Therefore, it is either nonmagnetic or antiferromagnetic. Figure 4(b) shows that the 1–4 and 1–6 dimers are antiferromagnetic. On the other hand the *ortho* and *para* dimmers are found nonmagnetic and are therefore not shown.

The first class of H dimers is related to non-Kekule structures. It involves the *meta*, 1–5, and 1–5 *bis* dimers and generally all the dimers where both H atoms are adsorbed on the same sublattice formed from *A* or *B* type carbon atom. In these cases, the second H atom is adsorbed at a low spin-density zone of the initial state (Fig. 3). The reactivity of the adsorbent carbon atom is here expected to be low since, from a local point of view, the $1s_2$ and χ_{1B} orbitals do not significantly overlap even when a common ring is concerned as in the case of the *meta* dimer. These dimers all involve carbon atoms of the same type and the resulting spin density in the final state is also borne by carbon atoms of the opposite type as shown in Fig. 4(a). The exchange energy is maximized when in the ferromagnetic state (local triplet state) since $E_x \sim \Sigma_j M_j^2$, where M_j stands for the magnetization.[4] From Table I, the ferromagnetic configuration ($\uparrow\uparrow$) is thus the most stable in all the non-Kekule dimers.

Dimers involving carbon atoms of different types are next investigated. We first consider the *ortho* or *para* configurations. From a local point of view, the unpaired electron of the second H atom interacts with a carbon atom on which the spin density of the initial state is strong; the $1s_2$ orbital centered on the second H atom and the χ_{1B} orbital strongly overlap. Electrons from each orbital pair covalently; a nonmagnetic state is formed. The electronic structure is spin unpolarized (restricted solution) and the spin density is zero everywhere in the supercell. The final state is nonmagnetic. On remote positions (1–4 and 1–6 dimers) the spin polarization decreases on the second adsorption site and the overlap between the $1s_2$ and χ_{1B} orbitals is much weaker. In the final state, spin polarization arises in two zones around each adsorption site [Fig. 4(b) unrestricted solutions]. Table I shows these configuration to be stable when antiferromagnetic.

The nonmagnetic and antiferromagnetic behaviors may be understood by establishing a correspondence between the related dimers and the H_2 molecule at small and large H-H distances, respectively. It is well known that at equilibrium and small H-H distances the spin density is zero on each H atom. On the other hand at large H-H distances the restricted description breaks down. The unrestricted description allows the spin-up and spin-down orbitals of the noninteracting system to be relaxed independently. It enables the $\rho\uparrow$ and $\rho\downarrow$ to be localized in different spatial regions as the result of the σ bond breaking between both H atoms. Such an unrestricted scheme delivers correct energies and correct spin density while of lower symmetry than that of the system.[31]

The *ortho*, *para*, and 1–4 to 1–6 dimers describe a similar situation to that just described for H_2: both H atoms are now
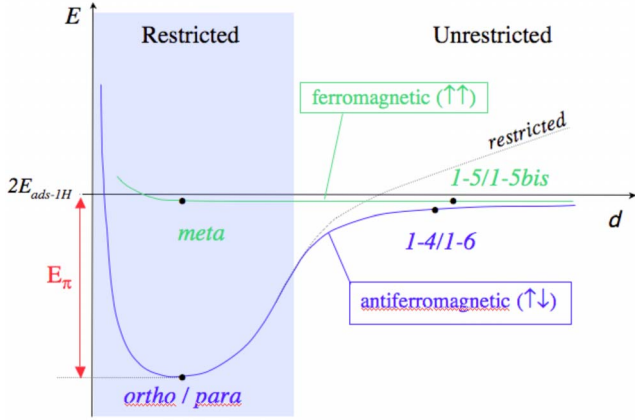
FIG. 6. (Color online) Schematic representation of the restricted and unrestricted energy solutions of dimers formed from different sublattice (in blue). The adsorption energies of the non-Kékulé dimers are also schematically shown in green (unrestricted solutions). The reference in energy is twice that of a single adsorption. The stabilization energy of the *ortho* and *para* dimers is E_π.

tied by a π bond that dissociates with increasing distance. The electronic structure of the *ortho* and *para* dimers is the counterpart of H-H at equilibrium and short distances leading to a nonmagnetic ($\uparrow\downarrow$) situation. Beyond these two dimers, the interaction between the two adsorption sites is weaker, the π bond dissociates while keeping the same spin configuration (Fig. 6); the solution is the counterpart of H-H at large distances with $\uparrow$ and $\downarrow$ densities localized in different spatial regions (Fig. 6).

2. Dimer stabilities

The whole adsorption process is now divided in some elementary steps. The single *H* adsorption involves (i) the breaking of an aromatic π bond with energy $E_{\pi \text{ bond}}$, then (ii) the adsorption of H on a *trigonal* carbon atom with formation of a C-H bond with energy E_H. This leaves an unpaired electron in the system

$$E_{\text{ads } 1H} = E_H - E_{\pi \text{ bond}}. \qquad (1)$$

Magnetic dimers are made of two distinct and nearly independent adsorption sites. The energy is twice that of a single adsorption:

$$E_{\text{ads } 2H} = 2E_H - 2E_{\pi \text{ bond}}. \qquad (2)$$

Putting aside the results from the *ortho* and *para* dimers, we estimate from Table I a mean adsorption energy of -65 kJ/mol *per* H atom on the basis of the periodic model. This is a good estimate since it agrees with the single H atom adsorption energy (-67 kJ/mol) value and also with the dimers adsorption energies which are calculated around -130 kJ/mol (1–4, 1–5, and 1–5 *bis* dimers).

In the *ortho* and *para* configurations, the second adsorption proceeds without breaking another π bond. As a result, the adsorption energy is

$$E_{\text{ads ortho-para}} = 2E_H - E_{\pi \text{ bond}}. \qquad (3)$$

The stabilization induced by these special configurations is $E_{p \text{ bond}}$. This result conveys an alternative view of what happens, namely, each H atom induces an aromatic π bond breaking upon adsorption and, at exclusively the *ortho* and *para* sites, an aromatic π bond is reconstructed.

Using the following mean values derived from Table I, $E_{\text{ads } 1H} = -65$ kJ mol^{-1}, $E_{\text{ads } 2H} = -130$ kJ mol^{-1}, and $E_{\text{ads ortho-para}} = -230$ kJ mol^{-1}, and solving Eqs. (1)–(3), we find:

$$E_H = -165 \text{ kJ/mol},$$

$$E_{\pi \text{ bond}} = -100 \text{ kJ/mol}.$$

The energy of formation of a π bond in alkenes is about 160 kJ mol^{-1}. However, in conjugated systems, the two unpaired electron resulting from the broken π bond strongly interact with the remaining π system. This interaction induces a strong stabilization in energy and the formation energy decreases to the range of $|E_{\pi \text{ bond}}|$ found above.

IV. DISCUSSION

The present work aimed at catching the essential features of the H dimers adsorption properties on graphitic systems. Graphene is not a graphite surface; some fine properties are sensitive to the interaction with underneath layers as, for example, the local density of states probed by STM.[8,32,33] However, as previously shown, graphene is a suitable model to investigate the H graphite interaction in the case of adsorption properties.[22] This assumption is here confirmed since our results are well consistent with the experimental results of Hornekær *et al.*[14] that showed the *ortho* and *para* dimers to be the most stable configurations on graphite.

The adsorption energies presently calculated for the seven different dimers are in good general agreement with the theoretical results of Refs. 16 and 34. However, the finding of Ref. 16 that nearest-neighbor carbon atoms relax below the surface is surprising. We have thus undertaken both periodic and molecular calculations with relaxation of the first and second-nearest-neighbor carbon atoms to investigate specifically this point. While these atoms do indeed relax they all move above the surface plane. For a single H atom adsorption site the out-of-plane position of the adsorbent C atom remains the same (0.39 Å) while its nearest neighbors move up by 0.05 Å. This result is consistent with previous ones obtained using different methods and models.[22,24,35] Therefore we expect these findings to remain the same for all the dimer cases considered except that of two adjacent adsorptions that are the *ortho* dimers. In this particular case the molecular calculations yield the following extra displacements: the adsorbent C atoms and their first neighbors move further up by 0.15 Å and the second-nearest neighbors by 0.05 Å. While these displacements are not negligible they change the *ortho* stabilization energy by only 7%. Aside from this feature the consistency of Table I and the conclusions drawn from it are not affected.

The main discrepancies with the work of Boukhvalov *et al.* concern magnetism. Both works agree with the ferromag-

netic properties of dimers involving carbon atoms of the same type in non-Kekule structures. Our work leads to a different conclusion as regards to the magnetic properties of the other dimers. The explanation of Boukhvalov *et al.* for the dimer stability is based on broken bonds. As a consequence, all dimers from different sublattices are nonmagnetic. Such a broken bond analysis would lead to rebuild a π bond between both adsorption sites, as for example, in the 1–4 dimer [Fig. 4(d) of Boukhvalov's paper]. However, this would induce an energy stabilization, which is found in neither works. Our finding using a broken-symmetry approach is that all the dimers involving carbon atoms of A and B types except the *ortho* and *para* ones are in an antiferromagnetic arrangement. Based on density maps, the interaction of both adsorption sites in the 1–4 dimer is weak and this dimer is antiferromagnetic. A π bond reconstruction as in the case of the *para* and *ortho* dimers cannot take place between the two distant and thereby weakly interacting adsorption sites; the adsorption energy of the 1–4 dimer is thus only twice that of a single adsorption.

Distance is not the only parameter determining the stability and magnetic properties of the dimer. Indeed, the adsorption sites interact more strongly in the 1–6 dimer than in the 1–4 one, leading to an increase in adsorption energy in the range of 30–40 kJ mol^{-1} (see Table I). This is tentatively attributed to the higher spin polarization seen in Fig. 3 in the 6 position as compared to that in the 4 one. This increase in adsorption energy is however less than one third of E_π. As a consequence, a π bond is not formed and spin polarization arises on both adsorption sites as shown in Fig. 4(b).

V. CONCLUSION

We have used a combination of molecular and periodic DFT approaches to investigate the basics of the H dimers adsorption on graphitic systems. As already observed, the *ortho* and *para* dimers exhibit an enhanced stability. This stability arises from the nonmagnetic properties of these dimers, which is a consequence of the formation of a π bond. The ferromagnetic and antiferromagnetic properties of the other dimers have also been put in evidence. This provides altogether a rationalization of the H dimer stabilities and magnetic properties. This comprehensive view has also enabled us to estimate the energetic values of the elementary H bonding and π bond breaking on graphite.

*yves.ferro@up.univ-mrs.fr

[1] L. Jeloaica and V. Sidis, Chem. Phys. Lett. **300**, 157 (1999).

[2] V. Sidis, L. Jeloaica, A. G. Borisov, and S. A. Deutscher, in *Molecular Hydrogen in Space*, Cambridge Contemporary Astrophysics Series, edited by F. Combes and G. Pineau des Forêts (Cambridge University Press, Cambridge, England, 2000), p. 89.

[3] P. Esquinazi, D. Spemann, R. Höhne, A. Setzer, K.-H. Han, and T. Butz, Phys. Rev. Lett. **91**, 227201 (2003).

[4] O. V. Yazyev and L. Helm, Phys. Rev. B **75**, 125408 (2007).

[5] D. Jiang, B. G. Sumpter, and S. Dai, J. Chem. Phys. **127**, 124703 (2007).

[6] Y. W. Soon, M. L. Cohen, and S. G. Louie, Nature (London) **444**, 347 (2006).

[7] H. Lee, N. Park, Y. W. Soon, S. Han, and J. Yu, Chem. Phys. Lett. **398**, 207 (2004).

[8] Y. Ferro and A. Allouche, Phys. Rev. B **75**, 155438 (2007).

[9] H. Amara, S. Latil, V. Meunier, P. Lambin, and J. C. Charlier, Phys. Rev. B **76**, 115423 (2007).

[10] Y. Zhang, S. Talapatra, S. Kar, R. Vajtai, S. K. Nayak, and P. M. Ajayan, Phys. Rev. Lett. **99**, 107201 (2007).

[11] Y. Ma, P. O. Lethinen, A. S. Foster, and R. M. Niemen, New J. Phys. **6**, 68 (2004).

[12] N. Rougeau, D. Teillet-Billy, and V. Sidis, Chem. Phys. Lett. **431**, 135 (2006).

[13] A. Allouche, Y. Ferro, T. Angot, C. Thomas, and J. M. Layet, J. Chem. Phys. **123**, 124701 (2005).

[14] L. Hornekær, Z. Sljivancanin, W. Xu, R. Otero, E. Rauls, I. Stensgaard, E. Lægsgaard, B. Hammer, and F. Besenbacher, Phys. Rev. Lett. **96**, 156104 (2006).

[15] A. Andree, M. Le Lay, T. Zecho, and J. Küpper, Chem. Phys. Lett. **425**, 99 (2006).

[16] D. W. Boukhvalov, M. I. Katsnelson, and A. I. Lichtenstein, Phys. Rev. B **77**, 035427 (2008).

[17] http://www.abinit.org

[18] J. P. Perdew, K. Burke, and M. Ernzerhof, Phys. Rev. Lett. **77**, 3865 (1996).

[19] N. Troullier and J. L. Martins, Phys. Rev. B **43**, 1993 (1991).

[20] H. J. Monkhorst and J. D. Pack, Phys. Rev. B **13**, 5188 (1972).

[21] J. C. Charlier, X. Gonze, and J. P. Michenaud, Phys. Rev. B **43**, 4579 (1991).

[22] Y. Ferro, F. Marinelli, and A. Allouche, J. Chem. Phys. **116**, 8124 (2002).

[23] X. Sha and B. Jackson, Surf. Sci. **496**, 318 (2002).

[24] Y. Ferro, F. Marinelli, and A. Allouche, Chem. Phys. Lett. **368**, 609 (2003).

[25] Amsterdam Density Functional, scientific computing and modelling (SCM), Theoretical Chemistry, Vrije Universiteit, Amsterdam, The Netherlands, http://www.scm.com

[26] J. P. Perdew, J. A. Chevary, S. H. Vosko, K. A. Jackson, M. R. Pederson, D. J. Singh, and C. Fiolhais, Phys. Rev. B **46**, 6671 (1992).

[27] M. B. Smith and J. March, *March's Advanced Organic Chemis-*

try: Reactions, Mechanisms, and Structure (Wiley, New York, 2007).

28 K. Goto, T. Kubo, K. Yamamoto, K. Nakasuji, K. Sato, D. Shiomi, T. Takui, M. Kubota, T. Kobayashi, K. Yakusi, and J. Ouyang, J. Am. Chem. Soc. **121** 1619 (1999).

29 J. Inoue, K. Fukui, T. Kubo, S. Nakazawa, K. Sato, D. Shiomi, Y. Morita, K. Yamamoto, T. Takui, and K. Nakasuji, J. Am. Chem. Soc. **123**, 12702 (2001).

30 Y. Ferro, F. Marinelli, A. Allouche, and C. Brosset, J. Chem. Phys. **118**, 5650 (2003).

31 W. Koch and M. C. Holthausen, in *A Chemist's Guide to Density Functional Theory* (Wiley, New York, 1999).

32 D. Tomanek, S. G. Louie, H. J. Mamin, and D. W. Abraham, Phys. Rev. B **35**, 7790 (1987).

33 D. Tomanek and S. G. Louie, Phys. Rev. B **37**, 8327 (1988).

34 T. Roman, W. A. Dino, H. Nakanishi, H. Kasai, T. Sugimoto, and K. Tange, Carbon **45**, 203 (2007).

35 Y. Ferro, F. Marinelli, A. Allouche, and C. Brosset, J. Nucl. Mater. **321**, 294 (2003).